Supplementary Information (SI) for Inorganic Chemistry Frontiers.

High entropy assisted platinum single atoms for photothermal green syngas production with high CO_2 utilization efficiency

Xin Liu[1, 6], Senyan Huang[1, 6], Dachao Yuan[1, 2, 6], Shan Li[3], Lin Ma[1], Linjie Gao[1*], Zhaoqi Li[1], Yachuan Wang[1], Yaguang Li [1, 2*], Jinhua Ye[1, 4, 5]

Experimental Section

Chemicals

Cerium nitrate ($Ce(NO_3)_3 \cdot 6H_2O$) was purchased from Kermel Co., Ltd. Polyvinylpyrrolidone(PVP), yttrium nitrate ($Y(NO)_3 \cdot 6H_2O$), lanthanum nitrate ($La(NO)_3 \cdot 6H_2O$), scandium nitrate hydrate ($Sc(NO_3)_3 \cdot H_2O$), zirconium nitrate ($Zr(NO_3)_4 \cdot 5H_2O$) were purchased from Macklin Co., Ltd. Chloroplatinic acid hexahydrate solution ($H_2PtCl_6 \cdot 6H_2O$) (1g/20ml), chloropalladated ammonium chloride($(NH_4)_2PdCl_6$), hexaammineruthenium trichloride ($Ru(NH_3)_6Cl_3$) were purchased from Shanghai Aladdin Biochemical Technology Co., Ltd. The chemicals were all used without any further treatment.

Synthesis of $CeYLaScZrO_x$

4 g PVP was dissolved in 20 ml H_2O. Then, 0.4503 g of $Ce(NO_3)_3 \cdot 6H_2O$, 0.3972 g of $Y(NO)_3 \cdot 6H_2O$, 0.4491 g of $La(NO)_3 \cdot 6H_2O$, 0.2582 g of $Sc(NO_3)_3 \cdot H_2O$ and 0.4452 g of $Zr(NO_3)_4 \cdot 5H_2O$ were added. The weight ratio of PVP/metal salts was 2. The solution was stirred for 1 hour and then dropped into liquid nitrogen to rapidly freeze to ice and lyophilized for 48 hours to remove H_2O. The dried sample was calcined in a muffle furnace for 6 hours at 700 °C (heating rate 1 °C per minute).

Synthesis of $Pt@CeYLaScZrO_x$

1 g of a prepared $CeYLaScZrO_x$ catalyst was added to 15 ml of deionized water and stirred. After stirring for 30 minutes 0.8 ml of $H_2PtCl_6 \cdot 6H_2O$ solution (1 g/20 ml) was added to the solution. After stirring for 4 hours, it was placed on a heated stirring table for stirring and drying. The drying temperature was set at 70 ℃. Finally, the dried sample was calcined in a muffle furnace to obtain $Pt@CeYLaScZrO_x$ catalyst. The calcination temperature was 700 ℃ and the rate of increase was 1 ℃ per minute.

$Pd@CeYLaScZrO_x$ and $Ru@CeYLaScZrO_x$ were synthesized according to the same procedures. The noble metal salts $(NH_4)_2PdCl_6$ and $Ru(NH_3)_6Cl_3$ were added in grams of 0.0517 g and 0.0459g, respectively.

Synthesis of ZrO_2, CeO_2, Y_2O_3, La_2O_3, Sc_2O_3.

4 g of PVP was dissolved in 20 ml of H_2O and then 2 g of $Zr(NO_3)_4 \cdot 5H_2O$ was added. The solution was stirred for 1 hour and then dropped into liquid nitrogen to rapidly freeze to ice and lyophilized for 48 hours to remove H_2O. The dried sample was calcined in a muffle furnace for 6 hours at 700 °C (heating rate 1 °C per minute).

CeO_2, Y_2O_3, La_2O_3, Sc_2O_3 were prepared in the same steps with the addition of 2 g of $Ce(NO_3)_3 \cdot 6H_2O$, $Y(NO_3)_3 \cdot 6H_2O$, $La(NO_3)_3 \cdot 6H_2O$ and $Sc(NO_3)_3 \cdot H_2O$, respectively.

Synthesis of Pt@ZrO_2, Pt@CeO_2, Pt@Y_2O_3, Pt@La_2O_3, Pt@Sc_2O_3.

1 g of a prepared ZrO_2 catalyst was added to 15 ml of deionized water and stirred. After stirring for 30 minutes 0.8 ml of $H_2PtCl_6 \cdot 6H_2O$ solution (1 g/20 ml) was added to the solution. After stirring for 4 hours it was placed on a heated stirring table for stirring and drying. The drying temperature was set at 70 °C. Finally, the dried sample was calcined in a muffle furnace to obtain Pt@ZrO_2 catalyst. The calcination temperature was 700 °C and the rate of increase was 1 °C per minute.

Pt@CeO_2, Pt@Y_2O_3, Pt@La_2O_3, Pt@Sc_2O_3 were prepared in the same steps with the addition of 1 g of catalyst, respectively.

The TiC/Cu-based device

Magnetron sputtering was used to deposit TiC/Cu film on reaction tube. TiC and Cu were used as the targets, and the working gas was Ar, which had 99.99% purity. Before the deposition process, the reaction tube was washed with deionized water, acetone, and ethanol subsequently, and then the glow-discharge was used to clean the reaction tube. The Cu layer and TiC film were orderly deposited on the surface of tube by magnetron sputtering of SP-0707AS. Specific parameters: the power was 4.5 KW, the sputtering pressure was 6×10^{-2} Pa, the bias voltage was 150 V, the sputtering temperature was 200 °C, and the sputtering time for Cu layer, TiC film was 16 min and 4 min, respectively. The following glass vacuum layer was provided by Hebei scientist research experimental and equipment trade Co., Ltd. with 1×10^{-3} Pa of pressure.

Characterizations

The TEM images are obtained on a JEOL2100plus transmission electron microscope operating at 200 kV. The samples are prepared by dropping water/ethanol

dispersion of samples onto ultrathin carbon film and immediately evaporating the solvent. The aberration-corrected high-angle annular dark-field scanning TEM (AC-HAADF-STEM) images and STEM-EDX elemental mapping are collected on a JEM-ARM200F transmission electron microscopy working at 200 kV, equipped with a probe spherical aberration corrector. The SEM images are acquired from FEI Nova Nano SEM450 scanning electron microscopes. XRD measurements of the obtained catalyst powders are performed on a Rigaku MiniFlex 600 diffractometer with a Cu-Kα X-ray radiation source (λ = 0.154056 nm). Typically, 2 mg of powders are placed on an amorphous silica substrate and the XRD patterns are record at a scan rate of 2° min^{-1}. XPS measurements are performed by a Thermo VG ESCALAB-250 system with Al-Kα and Mg-Kα source operated at 15 kV. The binding energies are referred to the C 1s peak (284.8 eV) from adventitious carbon. Zennium_Pro (Zahner, Germany) is an electrochemical workstation. N_2 sorption isotherms are measured at 77 K on a BELSORP MAX G absorption apparatus. Before tests, the samples are pre-activated at 120 °C for 12 h. The pore size distributions were estimated by the DFT method from a N_2 sorption experiment at 77 K. The metal content in our catalysts is determined by an ICP-OES spectrometer (Model Optima 2000, PerkinElmer). A series of solutions for the measurements are prepared by dissolving 20 mg of samples in 4 mL of aqua regia (75 vol.% HCl and 25 vol.% HNO_3). The solution is left overnight to allow complete dissolution. The resultant solution is diluted to 50 mL with deionized water in a volumetric flask and then analyzed using ICP-OES.

The Pd K-edge, Ru K-edge, Pt L-edge X-ray fine absorption structure data were collected on the beamline at Beijing Synchrotron and Shanghai Synchrotron Radiation Facility. All samples mixed with BN are coating on 3 M tape. A Si (111) crystal monochromator was used to filter the incident beam. We used IFEFFIT software to calibrate the energy scale, correct the background signal and normalize the intensity. In this work, the transmission mode was used to detect the Extended X-ray absorption fine structure of Ni K-edge and Ce L-edge. The spectra are normalized concerning the edge height after subtracting the pre- (-150 eV to -30 eV) and post-edge (50 eV to 800 eV)

backgrounds using Athena software.[1] To extract the EXAFS oscillations, the background was removed in k-space using a five-domain cubic spline.

First principle calculations

We have employed the Vienna Ab Initio Package (VASP)[2, 3] to perform all the density functional theory (DFT) calculations within the generalized gradient approximation (GGA) using the PBE formulation.[4] We have chosen the projected augmented wave (PAW) potentials[5, 6] to describe the ionic cores and take valence electrons into account using a plane wave basis set with a kinetic energy cutoff of 450 eV. Partial occupancies of the Kohn−Sham orbitals were allowed using the Gaussian smearing method and a width of 0.05 eV. The electronic energy was considered self-consistent when the energy change was smaller than 10^{-5} eV. A geometry optimization was considered convergent when the force change was smaller than 0.02 eV/Å. Grimme's DFT-D3 methodology was used to describe the dispersion interactions.[7]

The equilibrium lattice constant of ZrO_2 unit cell was optimized by using an 11×11×11 Monkhorst-Pack k-point grid for Brillouin zone sampling. We then use it to construct a ZrO_2(111) surface model (model 1) with *p*(4×3) periodicity in the X and Y directions and three stoichiometric layers in the Z direction by vacuum depth of 15 Å in order to separate the surface slab from its periodic duplicates. This model comprises of 36 Zr and 72 O atoms. Model 2 was built by 8 Ce atoms, 6 La atoms, 6 Sc atoms, 6 Y atoms, 10 Zr atoms and 63 O atoms into fluorite crystal cell. During structural optimizations, a 1×2×1 Brillouin zone was used for k-point sampling, and the bottom stoichiometric layer was fixed while the rest were allowed to fully relax. For the models of Pt single atoms, three Pt single atoms are bonded on the surface oxygens of Model 1 and Model 2. For the models of Pt clusters, three Pt atoms are stacked into cluster according to a face centered cubic structure on the surface of Model 1 and Model 2.

Thermocatalytic RWGS test

The thermocatalytic activity of catalysts for CO_2 hydrogenation is tested by the fixed-bed reactor (XM190708-007, DALIAN ZHONGJIARUILIN LIQUID TECHNOLOGY CO., LTD) in continuous flow form. 20 mg of catalysts are loaded in

a quartz tube for thermocatalytic RWGS test, the flow of feed gas is the mixture of 60 mL min^{-1} of H_2 and 20 mL min^{-1} of CO_2 . The reaction products are tested by gas chromatography (GC) 7890A equipped with FID and TCD detectors.

Photothermal RWGS

The photothermal RWGS is tested as follows: 1g of Pt@CEYLASCZTOX is loaded intoTiC/Cu based device (0.036 m^2), and irradiated by a light source (ZSL-4000). In this test, the flow of feed gas is the mixture of 90 mL min^{-1} of H_2 and 30 mL min^{-1} of CO_2. The reaction products are tested by gas chromatography (GC) 7890A equipped with FID and TCD detectors.

Table S1. CO_2 conversion rate of various catalysts in photothermal RWGS.

Catalyst	Light intensity (kW/m^2)	CO_2 conversion rate (%)	Refs.
$Pt@CeYLaScZrO_x$	3.2	45.6	This work
$Ni_1Ag_{0.02}O_1$	1	7.4	[8]
$Ni@p\text{-}SiO_2$	24	42	[9]
$5\%AgK/Fe_3O_4$	1	14.9	[10]
Fe_3O_4	52	19	[11]
CoFe-400	52	12.2	[11]
$Ru\text{-}Mo_2TiC_2$	38	2	[12]
Ir/Al_2O_3	None	14.94	[13]
$Pd@Nb_2O_5$	25	1.1	[14]
$Rh/In_2O_{3-x}(OH)_y$	9	9.55	[15]
CuZnAlCeZr	2	10.15	[16]
$Co\text{-}PS/SiO_2$	20	23	[17]
$BiO_x\text{-}CeO_2$	30	2.53	[18]
black In_2O_{3-x}	23	19.5	[19]
$Ni_{12}P_5/SiO_2$	23	1.5	[20]
Bi_2O_{3-x}	1.2	1.6	[21]
$Ni_{12}P_5@SiO_2$	40	4.3	[22]
$In_2O_{3-x}(OH)_y/SiNW$	20	0.1	[23]
$In_2O_{3-x}(OH)_y$ nanorods	8	0.5	[24]

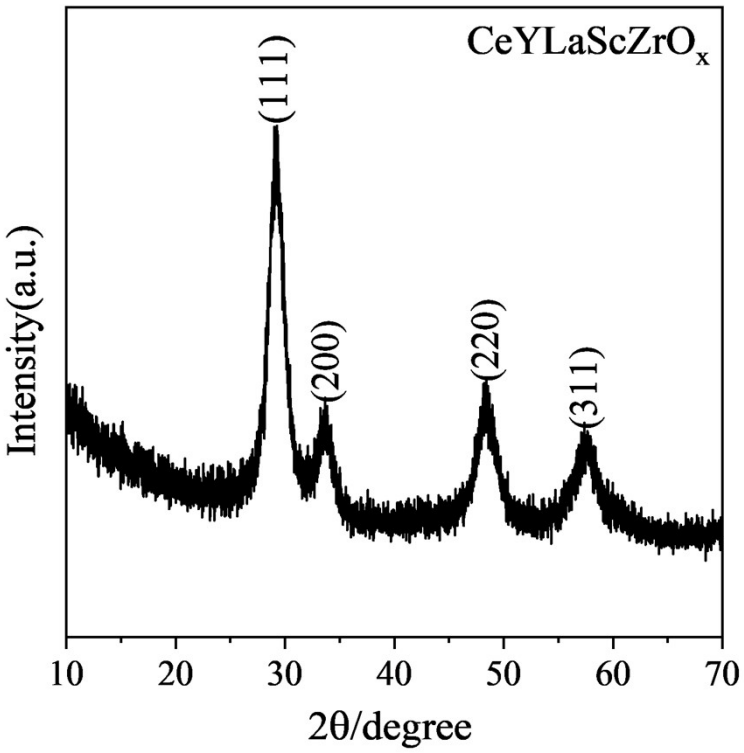

Fig. S1 XRD pattern of $CeYLaScZrO_x$.

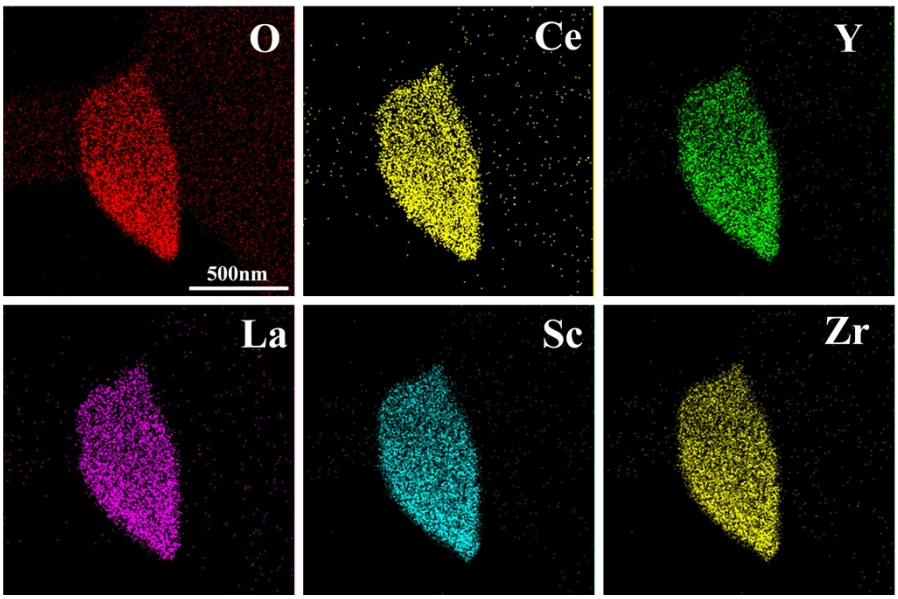

Fig. S2 O**,** Ce, Y, La, Sc, Zr elemental mapping images of $CeYLaScZrO_x$.

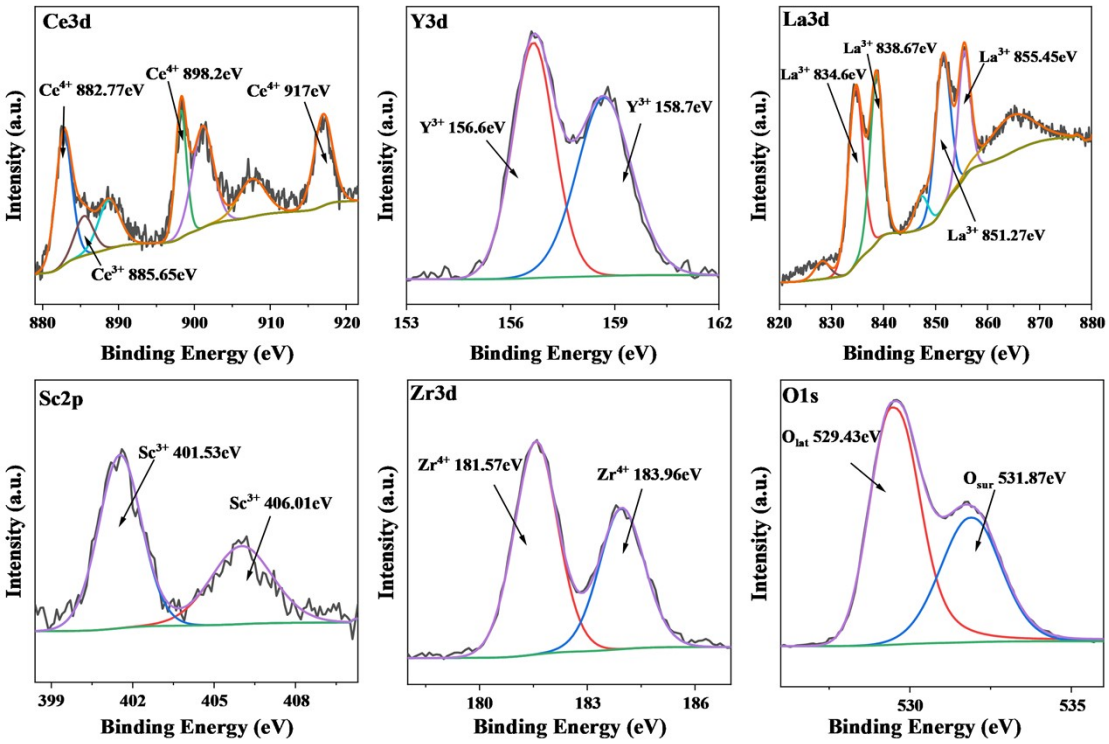

Fig. S3 Ce3d, Y3d, La3d, Sc2p, Zr3d, O1s XPS spectra of $CeYLaScZrO_x$.

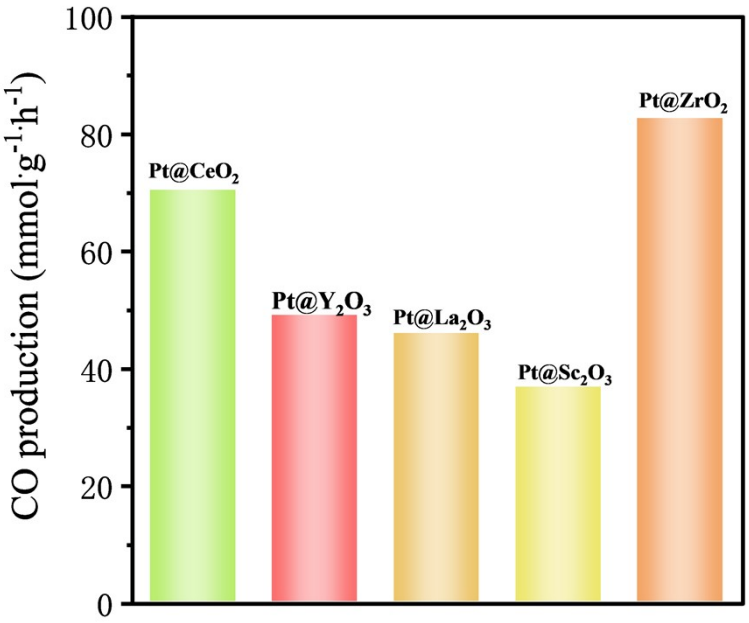

Fig. S4 CO production for the RWGS reaction at 450 ℃ over five catalysts. The RWGS test condition is: Catalysts' amount = 20 mg, H_2 flow rate = 60 mL min^{-1}, CO_2 flow rate = 20 mL min^{-1}, pressure=0.

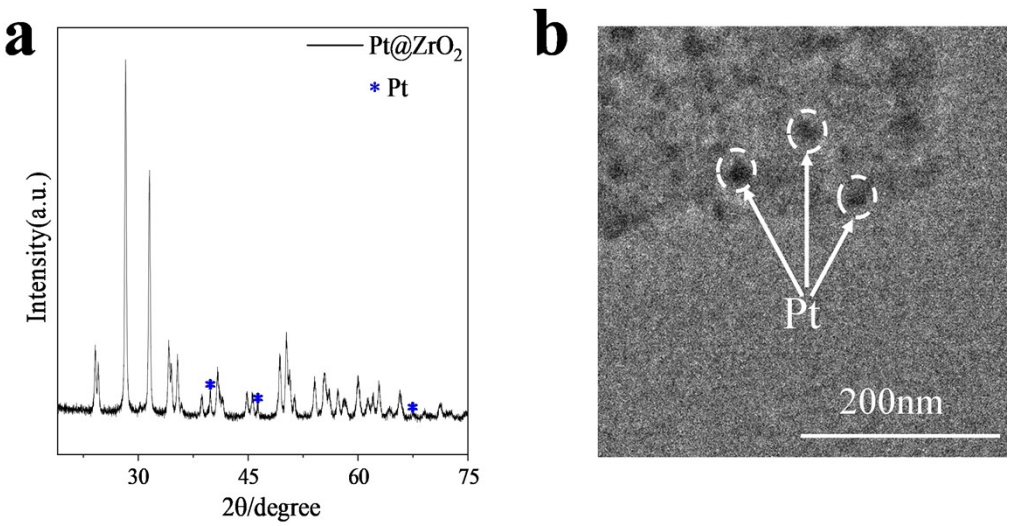

Fig. S5 (a) XRD pattern and (b) TEM image of $Pt@ZrO_2$.

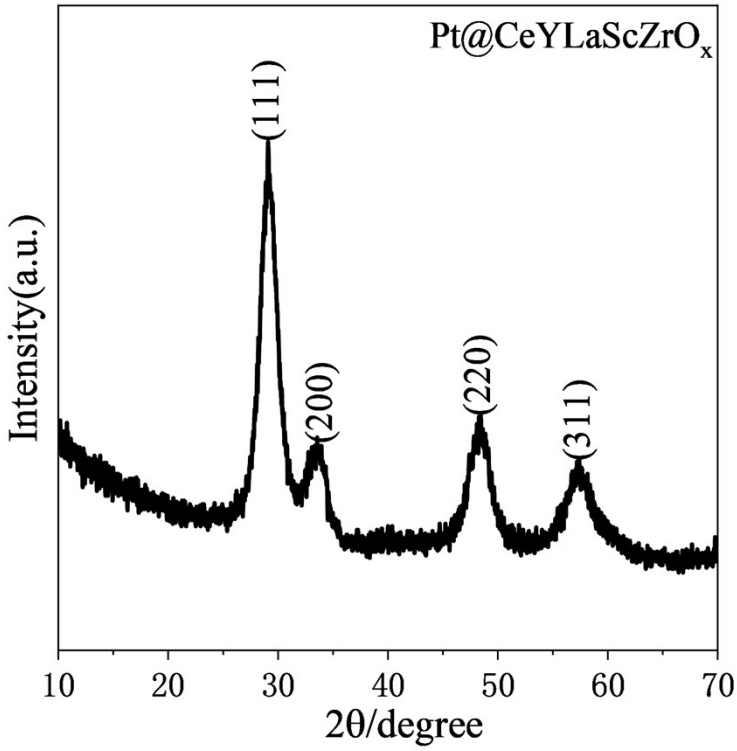

Fig. S6 XRD pattern of Pt@CeYLaScZrO$_x$.

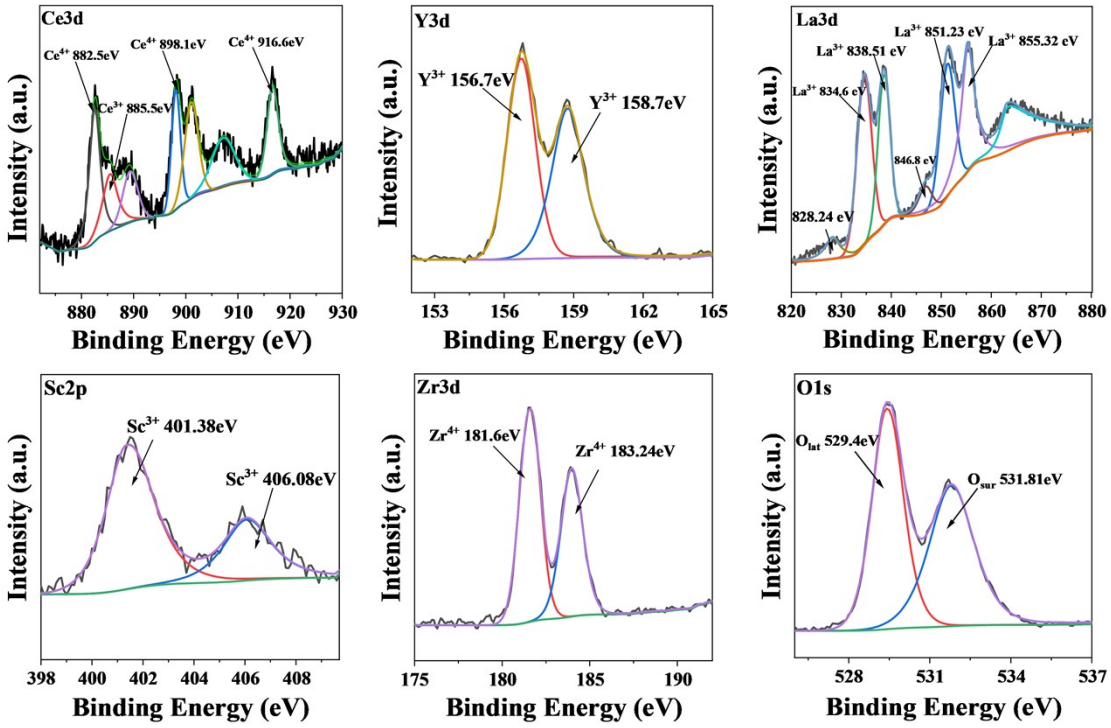

Fig. S7 Ce3d, Y3d, La3d, Sc2p, Zr3d, O1s XPS spectra of Pt@CeYLaScZrO_x.

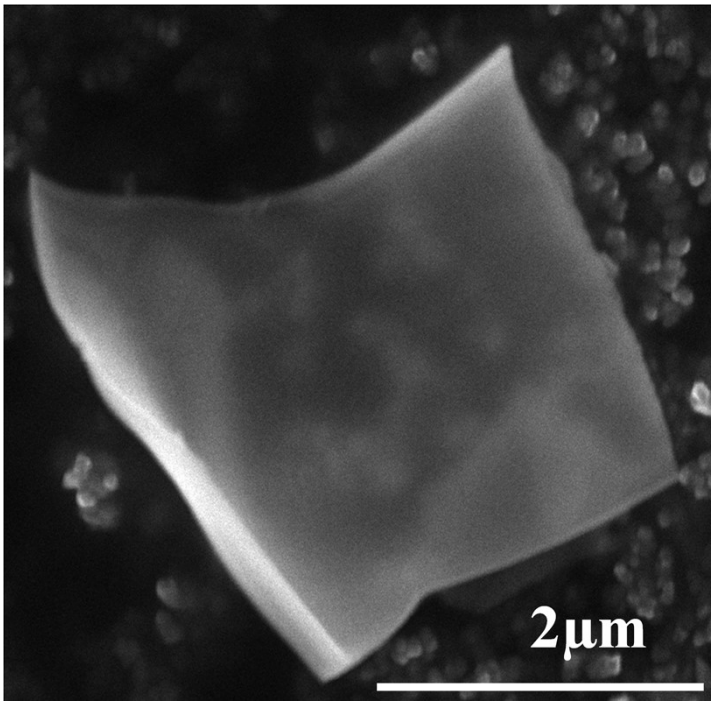

Fig. S8 SEM image of Pt@CeYLaScZrO_x.

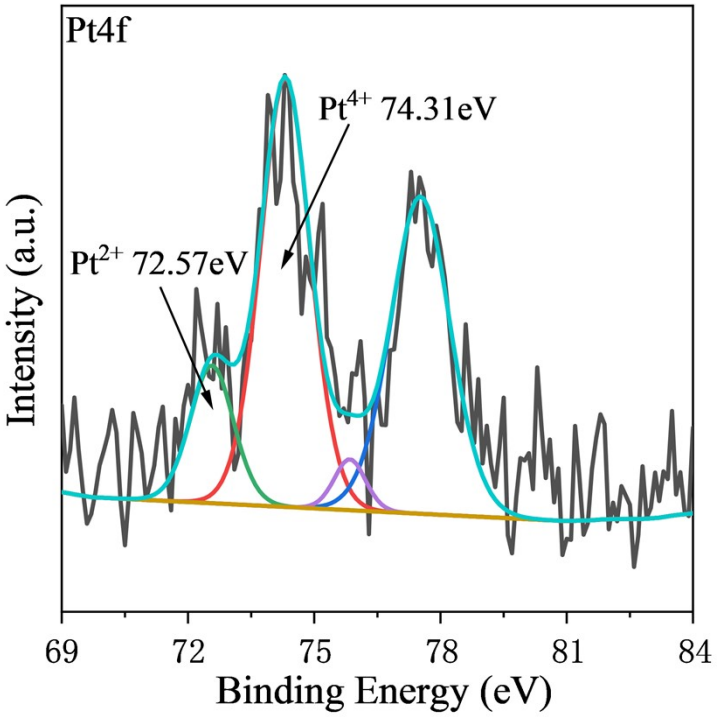

Fig. S9 Pt 4f XPS spectra of Pt@CeYLaScZrO_x.

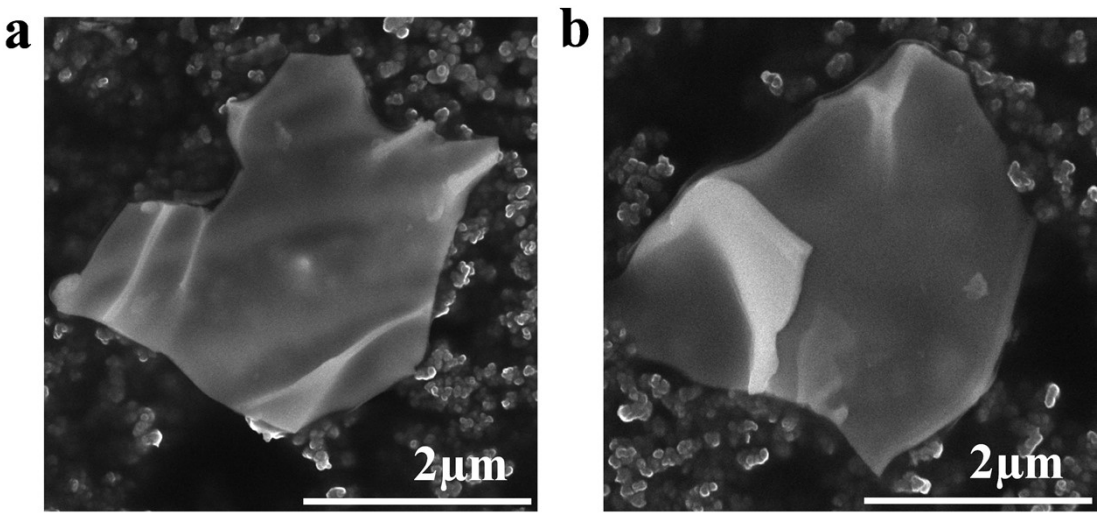

Fig. S10 SEM images of (a) Pd@CeYLaScZrO$_x$ and (b) Ru@CeYLaScZrO$_x$.

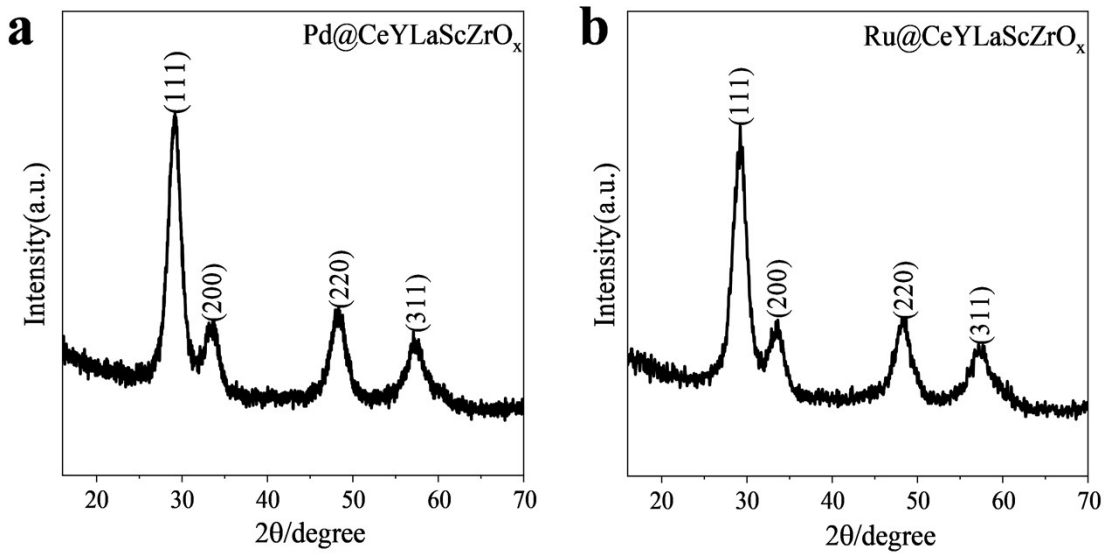

Fig. S11 XRD patterns of (a) Pd@CeYLaScZrO$_x$ and (b) Ru@CeYLaScZrO$_x$.

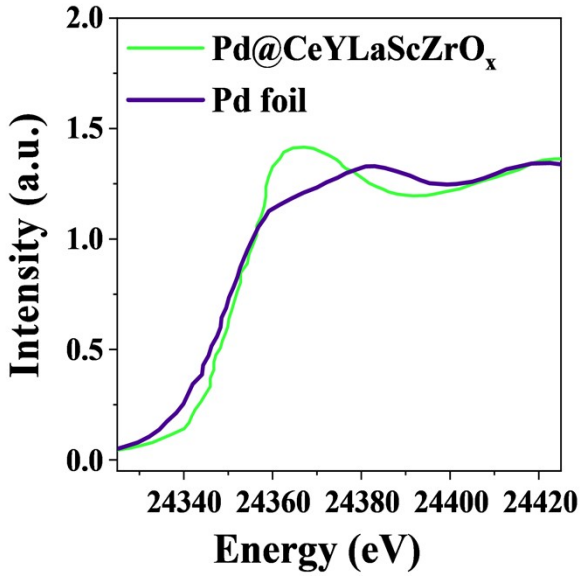

Fig. S12 XANES spectra at the Pd K-edge for Pd@CeYLaScZrO$_x$ and metallic Pd foil.

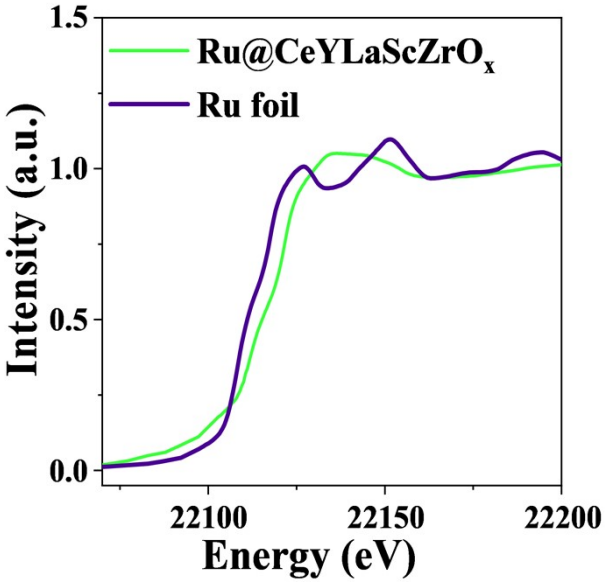

Fig. S13 XANES spectra at the Ru K-edge for Ru@CeYLaScZrO$_x$ and metallic Ru foil.

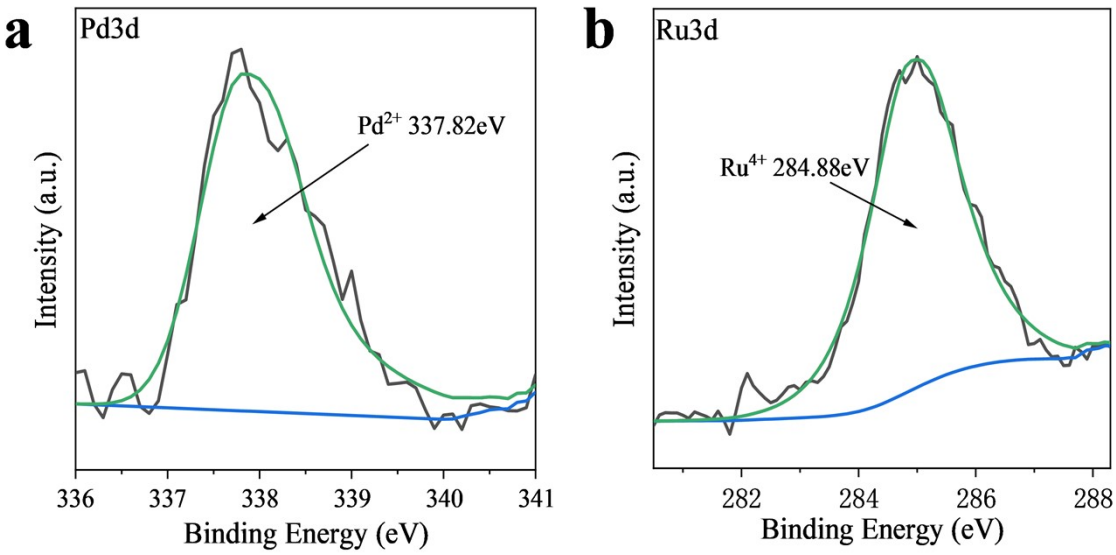

Fig. S14 (a) Pd 3d XPS spectra of Pd@CeYLaScZrO_x ,(b) Ru 3d XPS spectra of Ru@CeYLaScZrO_x.

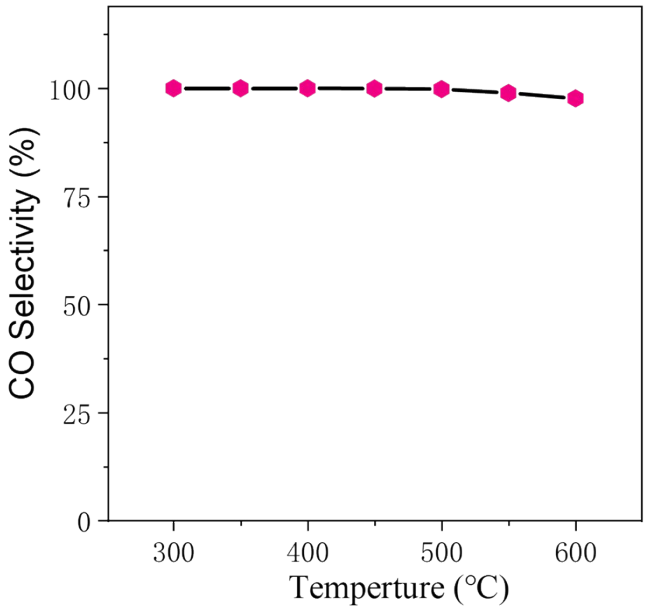

Fig. S15 CO selectivity of thermocatalytic RWGS over Pt@CeYLaScZrO_x.

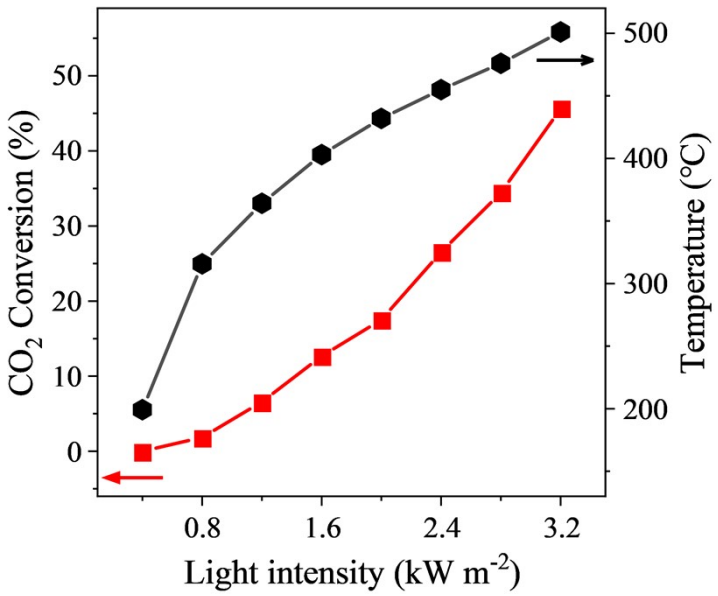

Fig. S16 CO_2 conversion rate of photothermal RWGS for Pt@CeYLaScZrO_x.

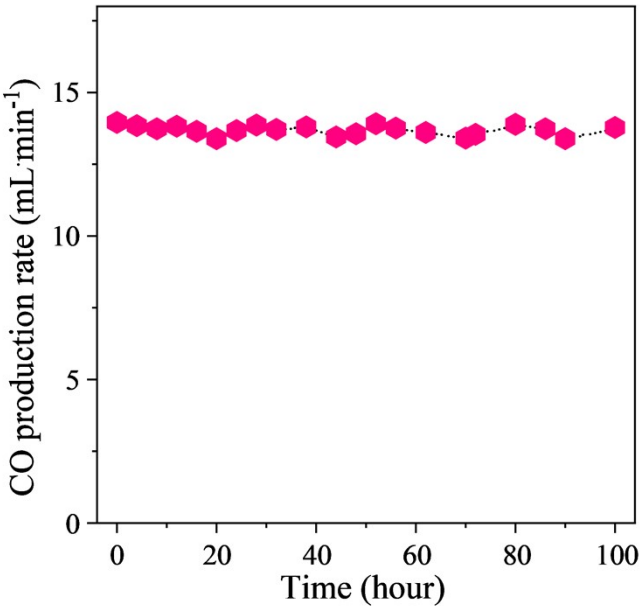

Fig. S17 CO production of photothermal RWGS for Pt@CeYLaScZrO$_x$ under 3.2 kW m^{-2} intensity of sunlight irradiation for 100 hours.

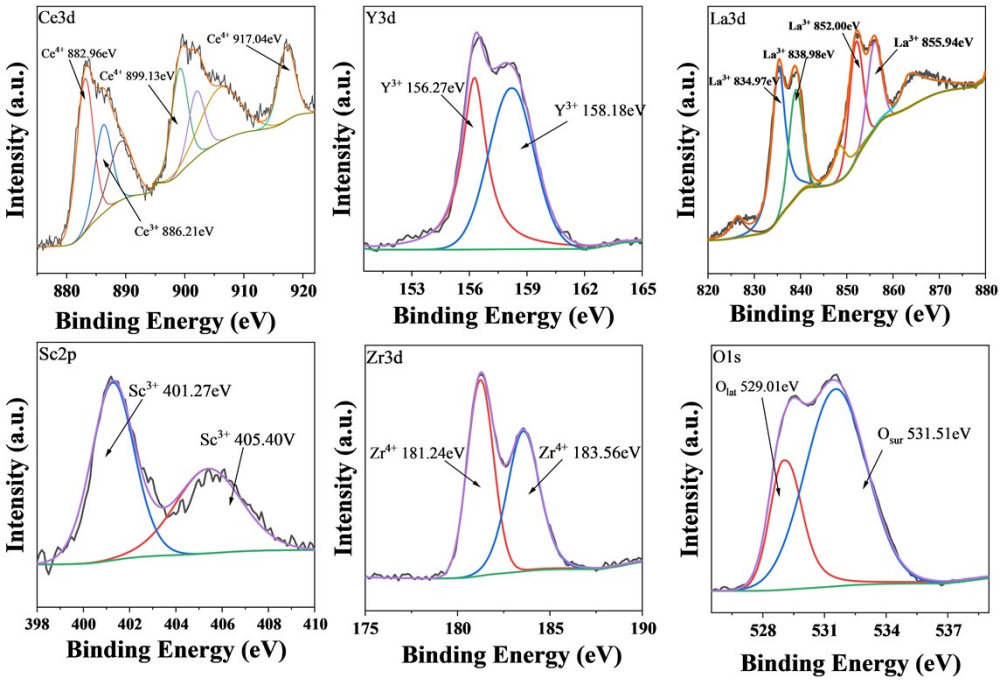

Fig. S18 Ce3d, Y3d, La3d, Sc2p, Zr3d, O1s XPS spectra of A-Pt@CeYLaScZrO_x.

References

1. B. Ravel and M. Newville, ARTEMIS, HEPHAESTUS: data analysis for X-ray absorption spectroscopy using IFEFFIT, *J. Synchrotron Radiat.*, 2005, **12**, 537-541.
2. G. Kresse and J. Furthmüller, Efficiency of ab-initio total energy calculations for metals and semiconductors using a plane-wave basis set, *Comput. Mater. Sci.*, 1996, **6**, 15-50.
3. G. Kresse and J. Furthmüller, Efficient iterative schemes for ab initio total-energy calculations using a plane-wave basis set, *Phys. Rev. B*, 1996, **54**, 11169-11186.
4. J. P. Perdew, K. Burke and M. Ernzerhof, Generalized Gradient Approximation Made Simple, *Phys. Rev. Lett.*, 1996, **77**, 3865-3868.
5. G. Kresse and D. Joubert, From ultrasoft pseudopotentials to the projector augmented-wave method, *Phys. Rev. B*, 1999, **59**, 1758-1775.
6. P. E. Blöchl, Projector augmented-wave method, *Phys. Rev. B*, 1994, **50**, 17953-17979.
7. S. Grimme, J. Antony, S. Ehrlich and H. Krieg, A consistent and accurate ab initio parametrization of density functional dispersion correction (DFT-D) for the 94 elements H-Pu, *J. Chem. Phys.*, 2010, **132**, 154104.
8. Y. Li, F. Meng, Q. Wu, D. Yuan, H. Wang, B. Liu, J. Wang, X. San, L. Gu and Q. Meng, A Ni-O-Ag photothermal catalyst enables 103-m^2 artificial photosynthesis with > 17% solar-to-chemical energy conversion efficiency, *Sci. Adv.*, 2024, **10**, eadn5098.
9. M. Cai, Z. Wu, Z. Li, L. Wang, W. Sun, A. A. Tountas, C. Li, S. Wang, K. Feng, A.-B. Xu, S. Tang, A. Tavasoli, M. Peng, W. Liu, A. S. Helmy, L. He, G. A. Ozin and X. Zhang, Greenhouse-inspired supra-photothermal CO_2 catalysis, *Nat. Energy*, 2021, **6**, 807-814.
10. Q. Wu, J. Wang, D. Yuan, Y. Wang, Y. Li, Y. Guo, Z. Zhang, X. San, L. Zhang and J. Ye, Ambient Sunlight Driven Photothermal Green Syngas Production at 100 m^3 Scale by the Dynamic Structural Reconstruction of Iron Oxides with 38.7% Efficiency, *Adv. Funct. Mater.*, 2025, **35**, 2412562.
11. G. Chen, R. Gao, Y. Zhao, Z. Li, G. I. N. Waterhouse, R. Shi, J. Zhao, M. Zhang, L. Shang, G. Sheng, X. Zhang, X. Wen, L. Z. Wu, C. H. Tung and T. Zhang, Alumina-Supported CoFe Alloy Catalysts Derived from Layered-Double-Hydroxide Nanosheets for Efficient Photothermal CO_2 Hydrogenation to Hydrocarbons, *Adv. Mater.*, 2018, **30,** 1704663.
12. Z. Wu, J. Shen, C. Li, C. Zhang, K. Feng, Z. Wang, X. Wang, D. M. Meira, M. Cai and D. Zhang, Mo_2TiC_2 MXene-supported Ru clusters for efficient photothermal reverse water–gas shift, *ACS Nano*, 2022, **17**, 1550-1559.
13. X. Meng, T. Wang, L. Liu, S. Ouyang, P. Li, H. Hu, T. Kako, H. Iwai, A. Tanaka and J. Ye, Photothermal Conversion of CO_2 into CH_4 with H_2 over Group VIII Nanocatalysts: An Alternative Approach for Solar Fuel Production, *Angew. Chem., Int. Ed.*, 2014, **53**, 11478-11482.
14. J. Jia, P. G. O'Brien, L. He, Q. Qiao, T. Fei, L. M. Reyes, T. E. Burrow, Y. Dong, K. Liao, M. Varela, S. J. Pennycook, M. Hmadeh, A. S. Helmy, N. P. Kherani, D. D. Perovic and G. A. Ozin, Visible and Near-Infrared Photothermal Catalyzed Hydrogenation of Gaseous CO_2 over Nanostructured Pd@Nb_2O_5, *Sci. Adv.*, 2016, **3**, 1600189.
15. T. Yan, L. Wang, Y. Liang, M. Makaremi, T. E. Wood, Y. Dai, B. Huang, F. M. Ali, Y. Dong and G. A. Ozin, Polymorph selection towards photocatalytic gaseous CO_2 hydrogenation, *Nat. Commun.*, 2019, **10**, 2521.
16. Y. Li, X. Bai, D. Yuan, C. Yu, X. San, Y. Guo, L. Zhang and J. Ye, Cu-based high-entropy two-dimensional oxide as stable and active photothermal catalyst, *Nat. Commun.*, 2023, **14**, 3171.

17. K. Feng, S. Wang, D. Zhang, L. Wang, Y. Yu, K. Feng, Z. Li, Z. Zhu, C. Li, M. Cai, Z. Wu, N. Kong, B. Yan, J. Zhong, X. Zhang, G. A. Ozin and L. He, Cobalt Plasmonic Superstructures Enable Almost 100% Broadband Photon Efficient CO_2 Photocatalysis, *Adv. Mater.*, 2020, **32,** 2000014.
18. X. Kang, D. Yuan, Z. Yi, C. Yu, X. Yuan, B. Liang, X. San, L. Gao, S. Wang and Y. Li, Bismuth single atom supported CeO_2 nanosheets for oxidation resistant photothermal reverse water gas shift reaction, *Catal. Sci. Technol.*, 2022, **12**, 5559-5564.
19. L. Wang, Y. Dong, T. Yan, Z. Hu, F. M. Ali, D. M. Meira, P. N. Duchesne, J. Y. Y. Loh, C. Qiu, E. E. Storey, Y. Xu, W. Sun, M. Ghoussoub, N. P. Kherani, A. S. Helmy and G. A. Ozin, Black indium oxide a photothermal CO_2 hydrogenation catalyst, *Nat. Commun.*, 2020, **11**, 2432.
20. Y.-F. Xu, P. N. Duchesne, L. Wang, A. Tavasoli, F. M. Ali, M. Xia, J.-F. Liao, D.-B. Kuang and G. A. Ozin, High-performance light-driven heterogeneous CO_2 catalysis with near-unity selectivity on metal phosphides, *Nat. Commun.*, 2020, **11**, 5149.
21. Y. Li, M. Wen, Y. Wang, G. Tian, C. Wang and J. Zhao, Plasmonic Hot Electrons from Oxygen Vacancies for Infrared Light-Driven Catalytic CO_2 Reduction on Bi_2O_{3-x}, *Angew. Chem.*, 2021, **133**, 923-929.
22. D. Lou, Z. Zhu, Y.-F. Xu, C. Li, K. Feng, D. Zhang, K. Lv, Z. Wu, C. Zhang and G. A. Ozin, A core-shell catalyst design boosts the performance of photothermal reverse water gas shift catalysis, *Sci. China Mater.*, 2021, **64**, 2212-2220.
23. L. B. Hoch, P. G. O'Brien, F. M. Ali, A. Sandhel, D. D. Perovic, C. A. Mims and G. A. Ozin, Nanostructured indium oxide coated silicon nanowire arrays: a hybrid photothermal/photochemical approach to solar fuels, *Acs Nano*, 2016, **10**, 9017-9025.
24. L. He, T. Wood, B. Wu, Y. Dong, L. Hoch, L. Reyes, D. Wang, C. Kübel, C. Qian and J. Jia, Spatial separation of charge carriers in $In_2O_{3-x}(OH)_y$ nanocrystal superstructures for enhanced gas-phase photocatalytic activity, *Acs Nano*, 2016, **10**, 5578-5586.